

Article

Synthesis of 1,3-Diols from Isobutene and HCHO via Prins Condensation-Hydrolysis Using CeO₂ Catalysts: Effects of Crystal Plane and Oxygen Vacancy

Zhixin Zhang ¹ , Yehong Wang ¹, Jianmin Lu ¹, Min Wang ¹, Jian Zhang ¹, Xuebin Liu ² and Feng Wang ^{1,*}

¹ State Key Laboratory of Catalysis, Dalian National Laboratory for Clean Energy, Dalian Institute of Chemical Physics, Chinese Academy of Sciences, Dalian 116023, China; zhangzhixin@dicp.ac.cn (Z.Z.); wangyehong@dicp.ac.cn (Y.W.); lujianmin@dicp.ac.cn (J.L.); wangmin@dicp.ac.cn (M.W.); zjian@dicp.ac.cn (J.Z.)

² Energy Innovation Laboratory, BP Office (Dalian Institute of Chemical Physics), Dalian 116023, China; xuebin.liu@se1.bp.com

* Correspondence: wangfeng@dicp.ac.cn; Tel.: +86-411-8437-9762

Received: 28 September 2017; Accepted: 2 November 2017; Published: 7 November 2017

Abstract: We herein report the synthesis of 3-methyl-1,3-butanediol from isobutene and HCHO in water via a Prins condensation-hydrolysis reaction over CeO₂, which is a water-tolerant Lewis acid catalyst. The CeO₂ exhibits significant catalytic activity for the reaction, giving 95% HCHO conversion and 84% 3-methyl-1,3-butanediol selectivity at 150 °C for 4 h. The crystal planes of CeO₂ have a significant effect on the catalytic activity for the Prins reaction. The (110) plane shows the highest catalytic activity among the crystal planes investigated (the (100), (110), and (111) planes), due to its higher concentration of Lewis acid sites, which is in line with the concentration of oxygen vacancies. Detailed characterizations, including NH₃-TPD, pyridine-adsorbed FT-IR spectroscopy, and Raman spectroscopy, revealed that the concentration of Lewis acid sites is proportional to the concentration of oxygen vacancies. This study indicates that the Lewis acidity induced by oxygen vacancy can be modulated by selective synthesis of CeO₂ with different morphologies, and that the Lewis acidity and oxygen vacancy play an important role in Prins condensation and hydrolysis reaction.

Keywords: CeO₂; crystal plane effect; Prins condensation; hydrolysis; oxygen vacancy; Lewis acidity

1. Introduction

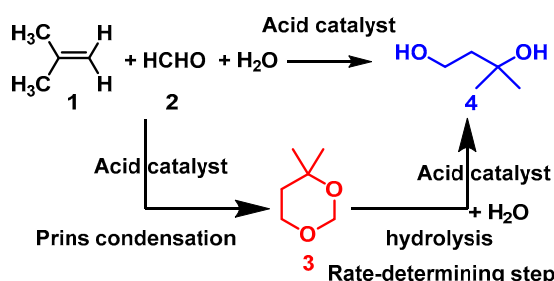
The Prins condensation of olefins with aldehydes is one of the most important organic reactions, allowing one to obtain alkyl-*m*-dioxanes, 1,3-diols, conjugated diolefins, and other valuable compounds [1,2]. Among these chemicals, 1,3-diols is a commodity chemical that is mainly used as a building block in polymerization and as a surfactant. For example, dehydration of 3-methyl-1,3-butanediol produces isoprene [3], which is mainly used as a monomer for manufacture of polyisoprene rubber and butyl rubber [4,5]. 3-methyl-1,3-butanediol can be synthesized by Prins condensation of isobutene with formaldehyde to 4,4-dimethyl-1,3-dioxane followed by its hydrolysis [6], which is a promising route because the feedstocks (isobutene [7–9] and formaldehyde [10,11]) can be found in bio-refineries, based on recent research and industrial progress [12–14]. In the synthesis route, both the Prins condensation and hydrolysis reaction require acid catalysts [3,15,16]. Various solid acid catalysts, such as metal oxide catalysts [17], zeolite catalysts [18], phosphate catalysts [15,19,20], and heteropolyacids catalysts [21,22], have been developed for the two-step reaction (Prins condensation and hydrolysis reaction). Alternatively, a single-stage 3-methyl-1,3-butanediol synthesis from isobutene and HCHO in water is one interesting route to be investigated, and a water-tolerant acid catalyst is critical.

Our previous work indicates that CeO_2 is a water-tolerant Lewis acid catalyst [23,24]. It has been proved that the coordinatively unsaturated Ce cations on CeO_2 surface act as the Lewis acid sites [25–28]. According to experimental data and theory calculations [24,29–32], the concentration of surface coordinatively unsaturated Ce cations is associated with the population of oxygen vacancies over CeO_2 . Additionally, the formation energy of oxygen vacancies varies greatly among different CeO_2 surfaces. For the three low-index surfaces of CeO_2 ((111), (110), and (100)), the formation energies of oxygen vacancy follow the order of (110) < (100) < (111) [33], which implies that the order of oxygen vacancy formation is (110) > (100) > (111). Therefore, selective synthesis of CeO_2 with different crystal planes would modulate the concentration of oxygen vacancies. Furthermore, the Lewis acidity of CeO_2 catalyst may be manipulated by morphology control.

In this study, 3-methyl-1,3-butanediol will be synthesized from isobutene and formaldehyde using CeO_2 catalysts via Prins condensation-hydrolysis reaction in water. CeO_2 with different morphologies (rod, octahedron, and cube) will be tested for the Prins condensation-hydrolysis reaction, and the effect of crystal planes ((111), (110), and (100)) and oxygen vacancy will also be investigated. $\text{NH}_3\text{-TPD}$, pyridine adsorption IR, and Raman spectroscopy were used to characterize the acid properties and defect structures of these CeO_2 catalysts. Based on these experiments, the structure-property-activity relationship will be established.

2. Results and Discussion

CeO_2 has been proved a highly active and water-tolerant catalyst for the synthesis of 1,3-butanediol from propylene and HCHO via Prins condensation-hydrolysis in water [24]. This work encouraged us to apply the CeO_2 catalyst for isobutene-formaldehyde condensation in water to synthesize 3-methyl-1,3-butanediol, which is an important higher-molecule alkanediol for the polymer industries; its synthesis is obviously difficult, but scientifically interesting. Our synthetic route includes the Prins condensation of isobutene with HCHO to 4,4-dimethyl-1,3-dioxane (3), and then hydrolysis of (3) to 3-methyl-1,3-butanediol (4) (Scheme 1).



Scheme 1. Prins condensation-hydrolysis of isobutene with HCHO in water.

2.1. Effect of Reaction Temperature

The Prins condensation-hydrolysis of isobutene with formaldehyde (FA) in water over pristine CeO_2 was conducted at different temperatures ranging from 60 to 150 °C for 4 h (Figure 1). It can be seen from Figure 1 that the FA conversion increases slowly from 1% at 60 °C to 13% at 100 °C and then rapidly increases to 95% at 150 °C. The total selectivities of 4,4-dimethyl-1,3-dioxane (3) and 3-methyl-1,3-butanediol (4) are above 98% throughout the temperature range (60–150 °C) investigated. No dehydration products (such as 3-methyl-butanol isomers and isoprene) [22,34] derived from 3-methyl-1,3-butanediol, which are usually obtained via vapor-phase dehydration at high temperatures (≥ 300 °C), were observed. In our catalytic system, the reactions were conducted at liquid phase (Reaction temperature ≤ 150 °C) and in water, which did not favor the dehydration of 3-methyl-1,3-butanediol. The selectivity of 4,4-dimethyl-1,3-dioxane (3) increases with increasing temperature below 130 °C, and then decreases with further increase in temperature; meanwhile, the selectivity of the target product, 3-methyl-1,3-butanediol (4), has the opposite behavior.

The hydrolysis of **3** to **4** seems to be the rate-determining step in the Prins condensation-hydrolysis reaction under our reaction conditions, and the high temperature ($>130\text{ }^{\circ}\text{C}$) favors the hydrolysis of 4,4-dimethyl-1,3-dioxane (**3**) to target product (**4**) (Scheme 1). These results show that the best yield (80%) of target product **4** can be achieved at $150\text{ }^{\circ}\text{C}$ among the reaction temperature range investigated.

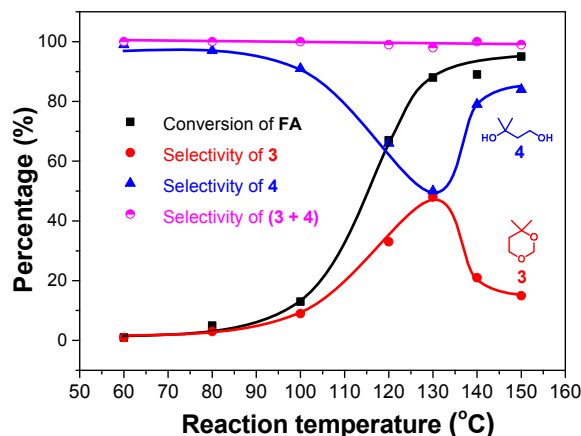


Figure 1. Effect of reaction temperature for the Prins condensation-hydrolysis of isobutene with FA in water over pristine CeO_2 . Reaction conditions: 50 mg CeO_2 , 1.5 mL H_2O , 0.21 mL HCHO (38 wt %), 3.0 g isobutene, 4 h.

2.2. Time-On-Stream Profile

Prins condensation-hydrolysis of isobutene with formaldehyde (FA) in water was conducted at $150\text{ }^{\circ}\text{C}$ over pristine CeO_2 to explore the optimal reaction time (Figure 2). The FA conversion rapidly increases to 95% after 4 h under the reaction conditions, and then levels off at ca. 95% with reaction times increased to 8 h. The highest selectivity of the target product 3-methyl-1,3-butanediol (**4**) is 84% during the time-on-stream investigated. Further increasing the reaction time, the selectivity of **4** seems to decrease slightly; simultaneously, the selectivities of **3** and others increase slightly. This behavior indicates the Prins condensation-hydrolysis reaction reaches equilibrium. The total selectivities of **3** and **4** are over 95% throughout the course of the reaction, and slightly decrease along with the increase in reaction time, indicating that side reactions may occur after long reaction times at such high temperature ($150\text{ }^{\circ}\text{C}$). These results indicate that pristine CeO_2 is a highly effective catalyst for the Prins condensation-hydrolysis reaction, and the best catalytic activity (95% FA conversion and 84% 3-methyl-1,3-butanediol selectivity) can be obtained at $150\text{ }^{\circ}\text{C}$ for 4 h.

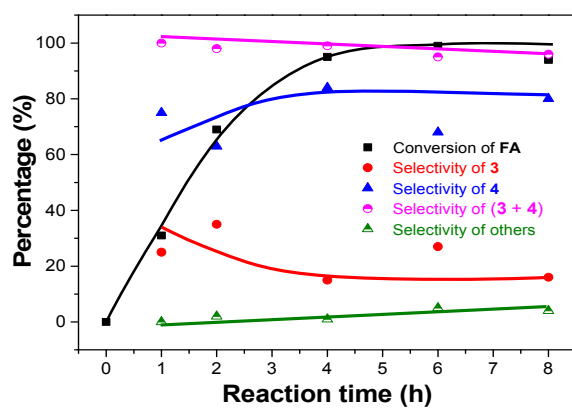


Figure 2. Reaction profiles for the Prins condensation-hydrolysis of isobutene with FA in water over pristine CeO_2 . Reaction conditions: 50 mg CeO_2 , 1.5 mL H_2O , 0.21 mL HCHO (38 wt %), 3.0 g isobutene, $150\text{ }^{\circ}\text{C}$.

2.3. Effect of Crystalline Plane

It has been reported that the exposed crystalline planes of CeO₂ (the (100), (110) and (111) crystalline planes) possess different surface concentrations of oxygen vacancies because of the difference in the formation energy of oxygen vacancies [29,35]. We successfully prepared CeO₂ with different morphologies via the previously reported methods [23,24,36,37], and confirmed their morphology by XRD (Figure S1) and HRTEM (Figure S2). The average sizes of CeO₂ with different morphologies were determined by TEM (Figure S2). The CeO₂-rods are about 7.4 nm in diameter and 69 nm in length, and the average sizes of CeO₂ octahedron and CeO₂-cube are 118 and 61 nm, respectively. Our studies [24,38,39] and others [33,40] have also proved that the nanorods, nanocubes, and nanoctahedrons of CeO₂ selectively expose (110) and (100), (100), and (111) planes, respectively (Table 1). The theoretical exposed crystalline planes and their ratio are shown in Table 1, as obtained from the literature [37].

Table 1. Prins condensation-hydrolysis of isobutene with FA in water over CeO₂ with different morphologies¹.

Entry	Catalyst	Exposed Crystalline Planes	Co A ₅₉₅ /A ₄₆₂ ²	S ⁴	Conv. (%)	Sel. (%)	
						3	4
1	CeO ₂ -rod	(110)/(100) = 2/1	0.077	86	32	13	87
2	CeO ₂ -cube	(100)	0.001	21	8	14	86
3	CeO ₂ -octahedron	(111)	0.003	9	1	12	88
4	Pristine CeO ₂	(111), (110), (100)	0.009 ³	67	13	9	91

¹ Reaction conditions: 50 mg catalyst, 1.5 mL H₂O, 0.21 mL HCHO (38 wt %), 3.0 g isobutene, 100 °C, 4 h. ² A₅₉₅/A₄₆₂ means the relative concentration of intrinsic oxygen vacancy concentration (Co) of CeO₂ samples determined by Raman spectra in Figure S3. ³ The A₅₉₅/A₄₆₂ value of pristine CeO₂ are referenced from literature [25]. ⁴ Specific surface area S_{BET} (m²·g⁻¹).

We tested the catalytic activities of CeO₂ with the three different morphologies in the Prins condensation-hydrolysis reaction, and the results are shown in Table 1. In order to distinguish the difference in catalytic performance of these three CeO₂ catalysts, relatively low reaction temperature (100 °C) was selected due to the similar catalytic activity of CeO₂ under harsh reaction conditions (such as 150 °C for 2 h) (Table S1). Under 100 °C for 4 h, 32% FA conversion and 87% 3-methyl-1,3-butanediol (**4**) selectivity were obtained for CeO₂-rod, meanwhile only 8% and 1% FA conversion were achieved for CeO₂-cube and CeO₂-octahedron with similar product distributions, respectively. For comparison, the catalytic activities of pristine CeO₂ (13% FA conversion and 91% 3-methyl-1,3-butanediol selectivity) were also listed in entry 4, Table 1. The order of catalytic activity is in line with the sequence of specific surface area (S_{BET}), which indicates that the S_{BET} is another key parameter for the catalytic performance over CeO₂. These results also indicate the CeO₂-rod is the best catalyst for the reaction among these catalysts. According to the exposed crystalline planes, we can conclude the (110) plane is the most active crystalline plane for this reaction.

As the complex crystal planes over the pristine CeO₂ surface, the well-defined CeO₂ with different morphologies were selected as models in this study to make clear the correlation between the catalytic performance and their physicochemical properties. NH₃-TPD, pyridine adsorption IR, and Raman spectroscopy were used to characterize the acid properties and oxygen-defect structures, respectively.

NH₃-TPD technique was used to investigate the acid strength of CeO₂ with different morphologies (Figure 3). All three CeO₂ samples have two broader NH₃-desorption peaks in the range from 50 to 600 °C in the desorption profiles. The high desorption peak around 110–156 °C can be ascribed to the weak acid sites, and the weak desorption peak centered at 340–420 °C is related to the medium acid sites on the CeO₂ surface. It can be found that these three samples mainly possess weak acid sites, along with a small number of medium ones. The two strongest peaks, at around 145 °C and 340 °C, which are ascribed to NH₃ adsorbed on weak acid sites and medium acid sites, respectively, were observed for CeO₂-rod. Two types of acid sites at low temperature around 110 °C and 156 °C and a

weak peak around 420 °C were observed for CeO₂-octahedron. Additionally, two weak peaks around 122 °C and 360 °C were detected for CeO₂-cube. Furthermore, the peak areas, which reflect the acidity, vary with the CeO₂ morphologies, and the CeO₂-rod catalyst shows the highest acidity among the three morphologies. These results also imply that the predominant factor responded for the different catalytic performance between the three catalysts may be the concentration of the acid sites.

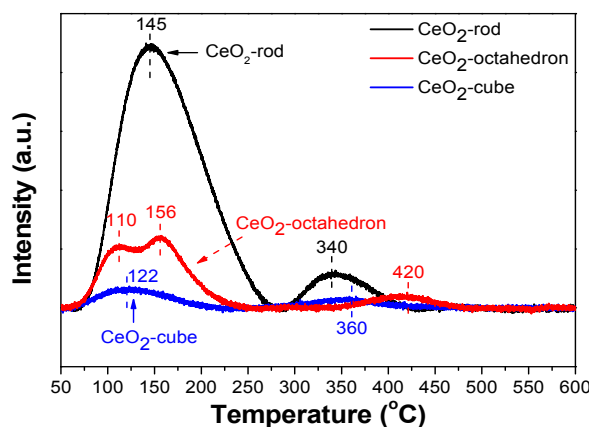


Figure 3. NH₃-TPD of CeO₂ with different morphologies.

Pyridine-adsorption IR is an effective characterization for measuring the concentration of the acid sites and distinguishing the acid type of solid catalysts [41–43]. From the pyridine adsorption IR spectra of CeO₂ with different morphologies (Figure 4), it can be seen that no characteristic band attributed to Brönsted acid sites, which usually appear around 1540 cm^{−1} [42], are observed on these samples. Strong bands around 1440 and 1595 cm^{−1} are observed, which are the characteristic bands of the coordinatively bound pyridine on Lewis acid sites [43]. The surface concentration of Lewis acid sites can be calculated based on the integrated band area at 1440 cm^{−1} and Formula (1) [44], and the CeO₂-rod presents the highest concentration of Lewis acid sites (188 μmol·g^{−1}), which is about threefold higher than that of CeO₂-octahedron (64 μmol·g^{−1}), and fivefold higher than that of CeO₂-cube (39 μmol·g^{−1}). Additionally, the concentration of Lewis acid sites over CeO₂-rod is 3.5 times higher than that of pristine CeO₂ (54 μmol·g^{−1}) [24,25]. We plot the concentration of Lewis acid sites and the catalytic performance versus the catalyst morphologies showed in Figure 5. It can be found that the CeO₂-rod obtains the best catalytic activity because of its higher Lewis acidity.

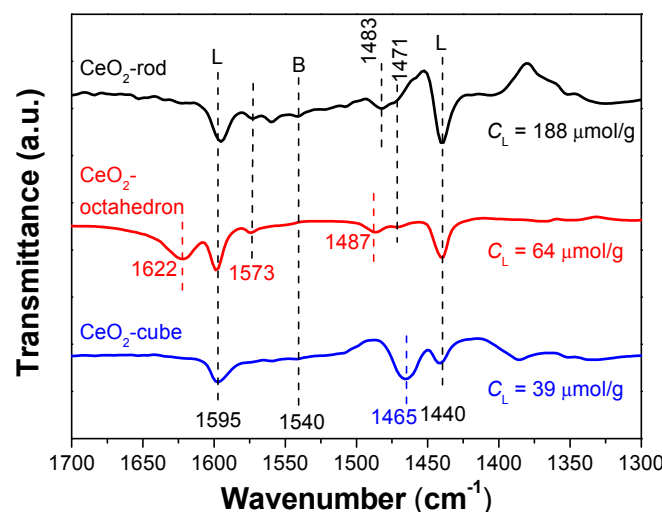


Figure 4. Pyridine adsorption IR spectra of CeO₂ with different morphologies.

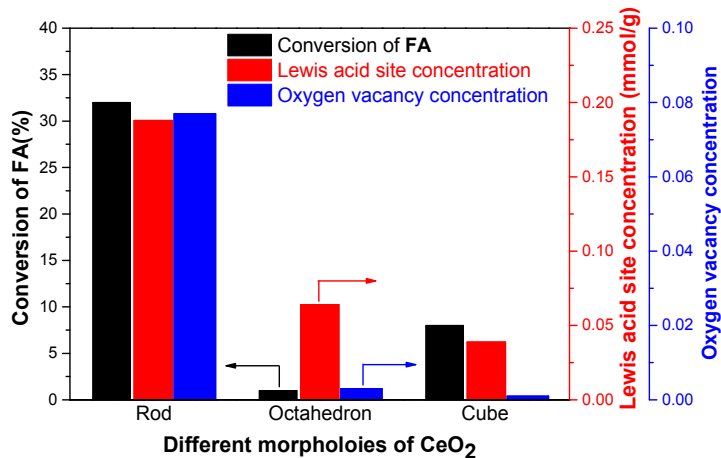


Figure 5. The relationship between the conversion of FA and the concentration of Lewis acid sites (unit: mmol/g) or the concentration of oxygen vacancies versus the CeO_2 with different morphologies.

It should be noted that some bands around 1622, 1573, 1485, and 1465 cm^{-1} were observed, which can be ascribed to the pyridine adsorbed on Lewis acid sites; these results indicate that the CeO_2 surface is predominately covered by Lewis acid sites. This result is in agreement with the previous study that only Lewis acid sites exist for CeO_2 [45,46] and metal-doped CeO_2 surfaces [25]. However, these complex bands imply the different Lewis acid sites for CeO_2 with different morphologies. The bands around 1573 and 1485 cm^{-1} for CeO_2 -rod and CeO_2 -octahedron surfaces are weak, and the influence on the concentration of Lewis acid sites may be neglected. However, the effect of 1622 and 1465 cm^{-1} on the concentration of Lewis acid sites should be considered, because these bands are obvious on the octahedron and cube, respectively. Furthermore, the peak area of 1465 cm^{-1} is larger than that of the 1622 cm^{-1} peak; this result may indicate that the concentration of Lewis acid sites over CeO_2 -cube is larger than that of CeO_2 -octahedron. This may be another reason for the opposite trend of HCHO conversion over CeO_2 -cube and octahedron when the conversion is correlated with the Lewis acid site concentration. Unfortunately, no consensus has been reached on the assignments of these bands, and the calculated formula has not yet been established. In the literature, the band at 1623 cm^{-1} could be assigned to the 8a mode for pyridine adsorbed on more acidic sites [47], but others have proposed that it is more likely to be due to the (1 + 6a) combination mode of pyridine [48]. The assignment of the 1465 cm^{-1} band is more complex. There are four assignments based on the literature [49]. Thus, more work is needed to assign and quantify these bands.

It is well known that the structure determines the performance. The above results spur us on to in-depth investigations of the CeO_2 structures with different morphologies. The surface oxygen of a perfect CeO_2 -rod, which exposes the (110) and (100) crystalline planes, is 9.5×10^{19} atom per gram, which is three-times (2.9×10^{19}) and seven-times (1.4×10^{19}) the values for a perfect cube and octahedron, respectively [23], implying the probability that oxygen vacancy formation for CeO_2 -rod is higher than that for cube and octahedron. DFT calculations have proven that the formation energies of oxygen vacancies for different CeO_2 surfaces follow the order of (110) < (100) < (111) [33], meaning that the order of intrinsic oxygen vacancy formation follows (110) > (100) > (111). Raman spectroscopy is a powerful technique for detecting the defect structures over metal oxides; here, we used it to determine the practical concentration of observed oxygen vacancies over the three CeO_2 catalysts. Figure S3 shows the visible (532 nm) Raman spectra of the CeO_2 samples with different morphologies, providing the information of several surface layers over CeO_2 . A strong band around 462 cm^{-1} and a weak band around 595 cm^{-1} were observed in all three samples. The former can be ascribed to the F_{2g} vibrational mode of CeO_2 , which possesses a fluorite-type structure [50]. The CeO_2 -rod gives a much broader 462 cm^{-1} peak than that of CeO_2 -octahedron and CeO_2 -cube, which is an inhomogeneous strain broadening caused by the differences in particle size between these three samples. This is

a size-dependent phenomenon observed on CeO_2 nanoparticles [51]. This is consistent with TEM measurement, where CeO_2 -rod has the smallest size among these three morphologies ($7.4 \text{ nm} \times 69 \text{ nm}$ for CeO_2 -rod, 118 nm for CeO_2 -octahedron, and 61 nm for CeO_2 -cube) (Figure S2). Interestingly, the HCHO conversion trend over these three morphologies is line with the particle size of these catalysts, indicating that the particle size may also affect the catalytic performance for the Prins reaction. The weak band around 595 cm^{-1} is related to intrinsic oxygen vacancy sites [52]. The oxygen vacancies detected by Raman spectroscopy are primarily those on several surface layers of the CeO_2 . The ratio of the integrated peak areas (A_{595}/A_{462}) was used to quantify the relative concentrations of oxygen vacancy [53]. The relative oxygen vacancy concentration of CeO_2 samples are shown in Table 1 and Figure S3. A plot of the oxygen vacancy concentration (measured by Raman spectra) and Lewis acid site concentration (measured by pyridine adsorption IR) against the catalyst morphologies was drawn (Figure 5). It can be found that the more oxygen vacancies, the more Lewis acid sites, and the CeO_2 -rod shows the highest concentration of oxygen vacancies and Lewis acid sites among the three morphologies.

Combined with the catalytic performances, Lewis acid site concentration, and oxygen vacancy concentration (Figure 5), we found an increase in FA conversion when changing the shape of CeO_2 . The CeO_2 -rod shows the best FA conversion because of its having the highest concentration of Lewis acid sites and oxygen vacancies among the three morphologies investigated.

It must be noted that the conversion trend does not seem to correlate with the concentration of Lewis acid sites and the number of oxygen vacancies for octahedrons and cubes. This may be caused by the following two factors: (1) the different specific surface area (S_A) between the CeO_2 -cube and octahedron (the S_A of CeO_2 -cube is $21 \text{ m}^2 \cdot \text{g}^{-1}$, which is 2.3-times higher than that of CeO_2 -octahedron, see Table 1); (2) the different particle sizes between CeO_2 -cube and octahedron (the particle size of CeO_2 -cube is about 61 nm , which is about 2-times larger than that of CeO_2 -octahedron ($\sim 118 \text{ nm}$), see Figure S2). The smaller and higher S_A of CeO_2 -cube could be attributed to the higher catalytic performance than that of CeO_2 -octahedron.

3. Materials and Methods

3.1. Materials

All chemicals and reagents were handled in air and used without further purification. $\text{Ce}(\text{NO}_3)_3 \cdot 6\text{H}_2\text{O}$ was of analytical grade (AR), obtained from Aladdin Chemicals. NaOH (AR), $\text{NH}_3 \cdot \text{H}_2\text{O}$ (28–30%), $\text{Na}_3\text{PO}_4 \cdot 12\text{H}_2\text{O}$ (99.5%), and HCHO (38 wt %) were obtained from Sinopharm Chemical Reagent Co., Ltd. (Shanghai, China).

3.2. Preparation of the CeO_2 Catalysts

Pristine CeO_2 were prepared by a traditional precipitation process described in the literature [23,24]. In a typical experiment, $\text{Ce}(\text{NO}_3)_3 \cdot 6\text{H}_2\text{O}$ (5.0 g) was dissolved in Millipore-purified water ($18 \text{ m}\Omega \cdot \text{cm}$, 100 mL), and then the solution was adjusted to a pH of 11.0 by the addition of $\text{NH}_3 \cdot \text{H}_2\text{O}$ under stirring at room temperature. The obtained precipitate was filtered, washed with deionized water, and then dried at 120°C for 12 h. The obtained solid was calcined at 500°C under the flow of air ($50 \text{ mL} \cdot \text{min}^{-1}$) for 4 h.

CeO_2 samples with different morphologies were prepared by hydrothermal methodology reported by our and other groups previously [23,24,36,37].

Preparation of CeO_2 -rod and cube. Typically, 5.209 g of $\text{Ce}(\text{NO}_3)_3 \cdot 6\text{H}_2\text{O}$ and a desired amount of NaOH (57.6–60 g) were dissolved in 20 mL and 210 mL of Millipore-purified water in a Teflon bottle, respectively. Then, the $\text{Ce}(\text{NO}_3)_3$ solution was added into the solution of NaOH under stirring at room temperature for 30 min, and a homogeneous milky slurry was formed. After the bottle was placed into a stainless steel vessel autoclave and sealed, the autoclave was heated to the desired temperature (100 – 180°C) in an oven for 24 h. After the hydrothermal treatment, the solution above the precipitate

was removed by centrifugation, and washed with deionized water and ethanol. Finally, the obtained sample was dried at 60 °C in an oven for 12 h.

Preparation of CeO₂-octahedron. Typically, 0.023 g of Na₃PO₄·12H₂O was added into the solution of Ce(NO₃)₃ (2.618 g in 240 mL of Millipore-purified water) under stirring at room temperature for 30 min in a Teflon bottle. Subsequently, the Teflon bottle was transferred into a stainless steel autoclave, and then placed in an oven at a temperature range of 170 °C for 12 h. After the hydrothermal treatment, the solution above the precipitate was removed by centrifugation, and washed with deionized water and ethanol. Finally, the obtained sample was dried at 60 °C in an oven for 12 h.

3.3. Prins Condensation-Hydrolysis Reaction

Aqueous formaldehyde (FA) (38 wt % HCHO, 0.21 mL, 3.0 mmol of HCHO), CeO₂ (50 mg), H₂O (1.5 mL), and a magnetic stir bar were loaded into a 15 ml Teflon-lined autoclave reactor. Quantified isobutene (99.99%) was charged into the reactor from a cylinder via weighting the reactor before and after the charging and then sealed. The sealed reactor was heated to the desired reaction temperature via a mantle. The 3-methyl-1,3-butanediol, 4,4-dimethyl-1,3-dioxane, etc., were analyzed by gas chromatography–mass spectrometry (GC–MS) using an Agilent 7890A/5975C (Santa Clara, CA, USA) instrument equipped with an HP-5MS column. The formaldehyde solution was analyzed by a GC (Tianmei, Shanghai, China) equipped with a packed column (GDX-401) and a TCD detector. An external standard was used to quantify the formaldehyde conversion.

3.4. Acidity Characterization by NH₃ Temperature-Programmed Desorption (NH₃-TPD)

The NH₃-TPD profiles of CeO₂ with different morphologies were recorded in a U-type quartz tube combined with an on-line mass spectrometer (MS, GSD320 Thermostar, Shanghai, China). In a typical experiment, about 40 mg of CeO₂ sample was placed in the tube and pretreated at 210 °C for 60 min under an argon flow (30 mL·min⁻¹), then cooling to 30 °C; several pulses of NH₃ were injected until no change in the NH₃ concentration was detected by the on-line MS. After that, the CeO₂ sample was flushed with argon for 60 min. Finally, the NH₃ desorption was conducted via increasing the oven temperature from 30 to 600 °C in the rate of 10 °C·min⁻¹. On-line MS recorded the gas effluents during the NH₃ desorption process.

3.5. Acidity Characterization by Pyridine Adsorption IR Spectroscopy

The acid type and concentration were determined by pyridine-adsorption IR spectra, which was conducted on a Bruker 70 IR spectrometer. A self-supporting sample disk of about 13 mm diameter (around 30 mg) was made by pressing in a mould, then the sample disk was placed into a homemade IR cell attached to a closed glass-circulation system. The disk was pretreated under a flow of argon (10 mL·min⁻¹) at 350 °C for 30 min, and then vacuumed for 30 min. After the temperature had cooled to 30 °C and the sample chamber had been evacuated to <10⁻³ mbar, a reference spectrum was recorded. After that, pyridine adsorption over sample disk was conducted via exposure to pyridine vapor. When the sample disk adsorbed pyridine was vacuumed at 150 °C for 30 min and cooled to 30 °C, the IR spectrum was recorded. The concentration of Lewis acid sites were calculated based on the integrated absorbance of the L band (1440 cm⁻¹) and the following formula [44]:

$$C = 1.42 \times IA \times R^2 / W \quad (1)$$

where C is the concentration of Lewis acid sites (mmol (g of catalyst)⁻¹), IA is the integrated absorbance of the L band (cm⁻¹), R is the radius of the catalyst disk (cm), and W is the mass of the sample disk (mg).

4. Conclusions

We demonstrate that CeO₂ is a highly effective catalyst for the synthesis of 1,3-diols from isobutene and HCHO via Prins condensation-hydrolysis reaction in water. 95% HCHO conversion

and 84% 3-methyl-1,3-butanediol selectivity were obtained over the pristine CeO_2 catalyst under 150 °C for 4 h. The crystal planes of CeO_2 have a significant effect on the catalytic activities for the condensation-hydrolysis reaction. The (110) plane over CeO_2 -rod surface is the most active crystalline plane for the reaction because of its having the richest intrinsic oxygen vacancies and highest Lewis acidity among the three low-index crystal planes investigated (the (100), (110), and (111) planes). Furthermore, the concentration of Lewis acid sites is proportional to the concentration of relative oxygen vacancies, indicating the strong contact between oxygen vacancies and Lewis acid sites. This study also implies that the Lewis acidity induced by oxygen vacancy can be modulate by the selective synthesis of CeO_2 with different crystal planes.

Supplementary Materials: The following are available online at www.mdpi.com/2304-6740/5/4/75/s1, Figure S1: XRD patterns of CeO_2 with different morphologies, Figure S2: TEM of (a) CeO_2 -rod; (b) CeO_2 -octahedron; and (c) CeO_2 -cube and HRTEM of (d) CeO_2 -rod; (e) CeO_2 -octahedron; and (f) CeO_2 -cube, Figure S3: Raman spectra of (a) CeO_2 -rod; (b) CeO_2 -octahedron; and (c) CeO_2 -cube, Table S1: Prins condensation-hydrolysis of isobutene with HCHO in water over CeO_2 with different morphologies.

Acknowledgments: This work was supported by the National Natural Science Foundation of China (21422308, 21403216 and 21690084), Strategic Priority Research Program of Chinese Academy of Sciences (XDB17020300), and by Dalian Institute of Chemical Physics (DICP DMTO201406).

Author Contributions: Zhixin Zhang and Feng Wang conceived and designed the experiments; Zhixin Zhang, Yehong Wang and Jian Zhang performed the experiments; Jianmin Lu and Min Wang analyzed the data; Xuebin Liu contributed reagents/materials/analysis tools; Zhixin Zhang, Xuebin Liu and Feng Wang wrote and revised the paper.

Conflicts of Interest: The authors declare no conflict of interest.

References

1. Isagulyants, V.I.; Khaimova, T.G.; Melikyan, V.R.; Pokrovskaya, S.V. Condensation of unsaturated compounds with formaldehyde (the Prins reaction). *Russ. Chem. Rev.* **1968**, *37*, 17–25. [[CrossRef](#)]
2. Arundale, E.; Mikeska, L.A. The olefin-aldehyde condensation. The Prins reaction. *Chem. Rev.* **1952**, *51*, 505–555. [[CrossRef](#)]
3. Ivanova, I.; Sushkevich, V.L.; Kolyagin, Y.G.; Ordomsky, V.V. Catalysis by coke deposits: Synthesis of isoprene over solid catalysts. *Angew. Chem. Int. Ed.* **2013**, *52*, 12961–12964. [[CrossRef](#)] [[PubMed](#)]
4. Chattopadhyay, D.K.; Raju, K.V.S.N. Structural engineering of polyurethane coatings for high performance applications. *Prog. Polym. Sci.* **2007**, *32*, 352–418. [[CrossRef](#)]
5. Fenouillot, F.; Rousseau, A.; Colomines, G.; Saint-Loup, R.; Pascault, J.P. Polymers from renewable 1,4:3,6-dianhydrohexitols (isosorbide, isomannide and isoiodide): A review. *Prog. Polym. Sci.* **2010**, *35*, 578–622. [[CrossRef](#)]
6. Yashima, T.; Katoh, Y.; Komatsu, T. Synthesis of 3-methyl-3-butene-1-ol from isobutene and formaldehyde on FeMCM-22 zeolites. In *Studies in Surface Science and Catalysis*; Kiricsi, I., Pál-Borbély, G., Nagy, J.B., Karge, H.G., Eds.; Elsevier: Amsterdam, The Netherlands, 1999; Volume 125, pp. 507–514.
7. Sun, J.; Zhu, K.; Gao, F.; Wang, C.; Liu, J.; Peden, C.H.; Wang, Y. Direct conversion of bio-ethanol to isobutene on nanosized $\text{Zn}_x\text{Zr}_y\text{O}_z$ mixed oxides with balanced acid-base sites. *J. Am. Chem. Soc.* **2011**, *133*, 11096–11099. [[CrossRef](#)] [[PubMed](#)]
8. Liu, C.; Sun, J.; Smith, C.; Wang, Y. A study of $\text{Zn}_x\text{Zr}_y\text{O}_z$ mixed oxides for direct conversion of ethanol to isobutene. *Appl. Catal. A* **2013**, *467*, 91–97. [[CrossRef](#)]
9. Sun, J.; Wang, Y. Recent advances in catalytic conversion of ethanol to chemicals. *ACS Catal.* **2014**, *4*, 1078–1090. [[CrossRef](#)]
10. Deo, G.; Wachs, I.E. Reactivity of supported vanadium-oxide catalysts—The partial oxidation of methanol. *J. Catal.* **1994**, *146*, 323–334. [[CrossRef](#)]
11. Routray, K.; Zhou, W.; Kiely, C.J.; Wachs, I.E. Catalysis science of methanol oxidation over iron vanadate catalysts: Nature of the catalytic active sites. *ACS Catal.* **2011**, *1*, 54–66. [[CrossRef](#)]
12. Martín, M.; Grossmann, I.E. Optimal simultaneous production of *i*-butene and ethanol from switchgrass. *Biomass Bioenergy* **2014**, *61*, 93–103. [[CrossRef](#)]

13. Crisci, A.J.; Dou, H.; Prasomsri, T.; Román-Leshkov, Y. Cascade reactions for the continuous and selective production of isobutene from bioderived acetic acid over zinc-zirconia catalysts. *ACS Catal.* **2014**, *4*, 4196–4200. [[CrossRef](#)]
14. De la Cruz, V.; Hernández, S.; Martín, M.; Grossmann, I.E. Integrated synthesis of biodiesel, bioethanol, isobutene, and glycerol ethers from algae. *Ind. Eng. Chem. Res.* **2014**, *53*, 14397–14407. [[CrossRef](#)]
15. Sushkevich, V.L.; Ordovsky, V.V.; Ivanova, I.I. Synthesis of isoprene from formaldehyde and isobutene over phosphate catalysts. *Appl. Catal. A* **2012**, *441*–442, 21–29. [[CrossRef](#)]
16. Sreevardhan Reddy, S.; David Raju, B.; Siva Kumar, V.; Padmasri, A.H.; Narayanan, S.; Rama Rao, K.S. Sulfonic acid functionalized mesoporous SBA-15 for selective synthesis of 4-phenyl-1,3-dioxane. *Catal. Commun.* **2007**, *8*, 261–266. [[CrossRef](#)]
17. Yamaguchi, T.; Nishimichi, C. Olefin-aldehyde condensation reaction on solid acids. *Catal. Today* **1993**, *16*, 555–562. [[CrossRef](#)]
18. Dumitriu, E.; Trong On, D.; Kaliaguine, S. Isoprene by Prins condensation over acidic molecular sieves. *J. Catal.* **1997**, *170*, 150–160. [[CrossRef](#)]
19. Krzywicki, A.; Wilanowicz, T.; Malinowski, S. Catalytic and physicochemical properties of the $\text{Al}_2\text{O}_3-\text{H}_3\text{PO}_4$ system, I. Vapor phase condensation of isobutylene and formaldehyde—The Prins reaction. *React. Kinet. Catal. Lett.* **1979**, *11*, 399–403. [[CrossRef](#)]
20. Ai, M. The formation of isoprene by means of a vapor-phase prins reaction between formaldehyde and isobutene. *J. Catal.* **1987**, *106*, 280–286. [[CrossRef](#)]
21. Li, G.; Gu, Y.; Ding, Y.; Zhang, H.; Wang, J.; Gao, Q.; Yan, L.; Suo, J. Wells–Dawson type molybdovanadophosphoric heteropolyacids catalyzed Prins cyclization of alkenes with paraformaldehyde under mild conditions—a facile and efficient method to 1,3-dioxane derivatives. *J. Mol. Catal. A Chem.* **2004**, *218*, 147–152. [[CrossRef](#)]
22. Songsiri, N.; Rempel, G.L.; Prasassarakich, P. Liquid-phase synthesis of isoprene from methyltert-butyl ether and formalin using Keggin-type heteropolyacids. *Ind. Eng. Chem. Res.* **2016**, *55*, 8933–8940. [[CrossRef](#)]
23. Wang, Y.H.; Wang, F.; Zhang, C.F.; Zhang, J.; Li, M.R.; Xu, J. Transformylating amine with DMF to formamide over CeO_2 catalyst. *Chem. Commun.* **2014**, *50*, 2438–2441. [[CrossRef](#)] [[PubMed](#)]
24. Wang, Y.H.; Wang, F.; Song, Q.; Xin, Q.; Xu, S.T.; Xu, J. Heterogeneous ceria catalyst with water-tolerant Lewis acidic sites for one-pot synthesis of 1,3-diols via Prins condensation and hydrolysis reactions. *J. Am. Chem. Soc.* **2013**, *135*, 1506–1515. [[CrossRef](#)] [[PubMed](#)]
25. Zhang, Z.; Wang, Y.; Lu, J.; Zhang, C.; Wang, M.; Li, M.; Liu, X.; Wang, F. Conversion of isobutene and formaldehyde to diol using praseodymium-doped CeO_2 catalyst. *ACS Catal.* **2016**, *6*, 8248–8254. [[CrossRef](#)]
26. Tamura, M.; Siddiki, S.; Shimizu, K. CeO_2 as a versatile and reusable catalyst for transesterification of esters with alcohols under solvent-free conditions. *Green Chem.* **2013**, *15*, 1641–1646. [[CrossRef](#)]
27. Tamura, M.; Sawabe, K.; Tomishige, K.; Satsuma, A.; Shimizu, K.-I. Substrate-specific heterogeneous catalysis of CeO_2 by entropic effects via multiple interactions. *ACS Catal.* **2015**, *5*, 20–26. [[CrossRef](#)]
28. Tamura, M.; Noro, K.; Honda, M.; Nakagawa, Y.; Tomishige, K. Highly efficient synthesis of cyclic ureas from CO_2 and diamines by a pure CeO_2 catalyst using a 2-propanol solvent. *Green Chem.* **2013**, *15*, 1567–1577. [[CrossRef](#)]
29. Paier, J.; Penschke, C.; Sauer, J. Oxygen defects and surface chemistry of ceria: Quantum chemical studies compared to experiment. *Chem. Rev.* **2013**, *113*, 3949–3985. [[CrossRef](#)] [[PubMed](#)]
30. Zhang, S.; Huang, Z.Q.; Ma, Y.; Gao, W.; Li, J.; Cao, F.; Li, L.; Chang, C.R.; Qu, Y. Solid frustrated-Lewis-pair catalysts constructed by regulations on surface defects of porous nanorods of CeO_2 . *Nat. Commun.* **2017**, *8*, 15266. [[CrossRef](#)] [[PubMed](#)]
31. Montini, T.; Melchionna, M.; Monai, M.; Fornasiero, P. Fundamentals and catalytic applications of CeO_2 -based materials. *Chem. Rev.* **2016**, *116*, 5987–6041. [[CrossRef](#)] [[PubMed](#)]
32. Sun, C.W.; Li, H.; Chen, L.Q. Nanostructured ceria-based materials: Synthesis, properties, and applications. *Energy Environ. Sci.* **2012**, *5*, 8475–8505. [[CrossRef](#)]
33. Si, R.; Flytzani-Stephanopoulos, M. Shape and crystal-plane effects of nanoscale ceria on the activity of Au- CeO_2 catalysts for the water-gas shift reaction. *Angew. Chem. Int. Ed.* **2008**, *47*, 2884–2887. [[CrossRef](#)] [[PubMed](#)]
34. Dumitriu, E.; Hulea, V.; Fechete, I.; Catrinescu, C.; Auroux, A.; Lacaze, J.-F.; Guimon, C. Prins condensation of isobutylene and formaldehyde over Fe-silicates of MFI structure. *Appl. Catal. A* **1999**, *181*, 15–28. [[CrossRef](#)]

35. Qiao, Z.A.; Wu, Z.L.; Dai, S. Shape-controlled ceria-based nanostructures for catalysis applications. *ChemSusChem* **2013**, *6*, 1821–1833. [CrossRef] [PubMed]
36. Wang, M.; Wang, F.; Ma, J.P.; Li, M.R.; Zhang, Z.; Wang, Y.H.; Zhang, X.C.; Xu, J. Investigations on the crystal plane effect of ceria on gold catalysis in the oxidative dehydrogenation of alcohols and amines in the liquid phase. *Chem. Commun.* **2014**, *50*, 292–294. [CrossRef] [PubMed]
37. Mai, H.X.; Sun, L.D.; Zhang, Y.W.; Si, R.; Feng, W.; Zhang, H.P.; Liu, H.C.; Yan, C.H. Shape-selective synthesis and oxygen storage behavior of ceria nanopolyhedra, nanorods, and nanocubes. *J. Phys. Chem. B* **2005**, *109*, 24380–24385. [CrossRef] [PubMed]
38. Zhang, Z.; Wang, Y.; Wang, M.; Lu, J.; Zhang, C.; Li, L.; Jiang, J.; Wang, F. The cascade synthesis of α,β -unsaturated ketones via oxidative C–C coupling of ketones and primary alcohols over a ceria catalyst. *Catal. Sci. Technol.* **2016**, *6*, 1693–1700. [CrossRef]
39. Zhang, Z.; Wang, Y.; Wang, M.; Lü, J.; Li, L.; Zhang, Z.; Li, M.; Jiang, J.; Wang, F. An investigation of the effects of CeO₂ crystal planes on the aerobic oxidative synthesis of imines from alcohols and amines. *Chin. J. Catal.* **2015**, *36*, 1623–1630. [CrossRef]
40. Huang, X.S.; Sun, H.; Wang, L.C.; Liu, Y.M.; Fan, K.N.; Cao, Y. Morphology effects of nanoscale ceria on the activity of Au/CeO₂ catalysts for low-temperature CO oxidation. *Appl. Catal. B* **2009**, *90*, 224–232. [CrossRef]
41. Parry, E.P. An infrared study of pyridine adsorbed on acidic solids. Characterization of surface acidity. *J. Catal.* **1963**, *2*, 371–379. [CrossRef]
42. Chakraborty, B.; Viswanathan, B. Surface acidity of MCM-41 by in situ IR studies of pyridine adsorption. *Catal. Today* **1999**, *49*, 253–260. [CrossRef]
43. Tamura, M.; Shimizu, K.-I.; Satsuma, A. Comprehensive IR study on acid/base properties of metal oxides. *Appl. Catal. A* **2012**, *433–434*, 135–145. [CrossRef]
44. Emeis, C.A. Determination of integrated molar extinction coefficients for infrared absorption bands of pyridine adsorbed on solid acid catalysts. *J. Catal.* **1993**, *141*, 347–354. [CrossRef]
45. Tamura, M.; Wakasugi, H.; Shimizu, K.; Satsuma, A. Efficient and substrate-specific hydration of nitriles to amides in water by using a CeO₂ catalyst. *Chem. Eur. J.* **2011**, *17*, 11428–11431. [CrossRef] [PubMed]
46. Wu, Z.; Mann, A.K.P.; Li, M.; Overbury, S.H. Spectroscopic investigation of surface-dependent acid–base property of ceria nanoshapes. *J. Phys. Chem. C* **2015**, *119*, 7340–7350. [CrossRef]
47. Zaki, M.I.; Hussein, G.A.M.; Mansour, S.A.A.; El-Ammawy, H.A. Adsorption and surface reactions of pyridine on pure and doped ceria catalysts as studied by infrared spectroscopy. *J. Mol. Catal.* **1989**, *51*, 209–220. [CrossRef]
48. Binet, C.; Daturi, M.; Lavallee, J.-C. IR study of polycrystalline ceria properties in oxidised and reduced states. *Catal. Today* **1999**, *50*, 207–225. [CrossRef]
49. Flego, C.; Kiricsi, I.; Perego, C.; Bellussi, G. The Origin of the Band at 1462 cm^{−1} Generally Appearing Upon Desorption of Pyridine from Acidic Solids—Steps Towards a More Comprehensive Understanding. *Catal. Lett.* **1995**, *35*, 125–133. [CrossRef]
50. Shyu, J.Z.; Weber, W.H.; Gandhi, H.S. Surface characterization of alumina-supported ceria. *J. Phys. Chem.* **1988**, *92*, 4964–4970. [CrossRef]
51. Wu, Z.; Li, M.; Howe, J.; Meyer, H.M.; Overbury, S.H. Probing defect sites on CeO₂ nanocrystals with well-defined surface planes by Raman spectroscopy and O₂ adsorption. *Langmuir* **2010**, *26*, 16595–16606. [CrossRef] [PubMed]
52. Popovic, Z.V.; Dohcevic-Mitrovic, Z.; Konstantinovic, M.J.; Scepanovic, M. Raman scattering characterization of nanopowders and nanowires (rods). *J. Raman Spectrosc.* **2007**, *38*, 750–755. [CrossRef]
53. Li, L.; Chen, F.; Lu, J.Q.; Luo, M.F. Study of defect sites in Ce_{1-x}M_xO_{2-δ} ($x = 0.2$) solid solutions using Raman spectroscopy. *J. Phys. Chem. A* **2011**, *115*, 7972–7977. [CrossRef] [PubMed]

